IEEE Access
Multidisciplinary | Rapid Review | Open Access Journal

Received 8 December 2023, accepted 21 December 2023, date of publication 1 January 2024,
date of current version 9 January 2024.

Digital Object Identifier 10.1109/ACCESS.2023.3348786

RESEARCH ARTICLE

Novel Ultra-Compact Wide Stopband Microstrip Lowpass-Bandpass Triplexer for 5G Multi-Service Wireless Networks

LEILA NOURI[1,2], FARID ZUBIR[3], (Member, IEEE), LEWIS NKENYEREYE[4], ABBAS REZAEI[5], MOHAMMED ABDEL-HAFEZ[6], (Senior Member, IEEE), FAWWAZ HAZZAZI[7], MUHAMMAD AKMAL CHAUDHARY[8], (Senior Member, IEEE), MAHER ASSAAD[8], AND ZUBAIDA YUSOFF[9], (Senior Member, IEEE)

[1]Institute of Research and Development, Duy Tan University, Da Nang 50000, Vietnam
[2]School of Engineering and Technology, Duy Tan University, Da Nang 50000, Vietnam
[3]Wireless Communication Centre, Faculty of Electrical Engineering, Universiti Teknologi Malaysia, Johor Bahru, Johor 81310, Malaysia
[4]Department of Computer and Information Security, Sejong University, Seoul 05006, South Korea
[5]Department of Electrical Engineering, Kermanshah University of Technology, Kermanshah 67146, Iran
[6]Department of Electrical and Communication Engineering, United Arab Emirates University, Al Ain, United Arab Emirates
[7]Department of Electrical Engineering, College of Engineering, Prince Sattam bin Abdulaziz University, Al-Kharj 11492, Saudi Arabia
[8]Department of Electrical and Computer Engineering, College of Engineering and Information Technology, Ajman University, Ajman, United Arab Emirates
[9]Faculty of Engineering, Multimedia University, Persiaran Multimedia, Cyberjaya, Selangor 63100, Malaysia

Corresponding authors: Farid Zubir (faridzubir@utm.my), Lewis Nkenyereye (nkenyele@sejong.ac.kr), and Zubaida Yusoff (zubaida@mmu.edu.my)

This work was supported in part by the Higher Institution Centre of Excellence (HICOE), Ministry of Higher Education Malaysia, through the Wireless Communication Centre (WCC), Universiti Teknologi Malaysia (UTM) under Grant R.J090301.7823.4J610; and in part by the Faculty of Engineering, Multimedia University (MMU), Cyberjaya, Malaysia.

ABSTRACT This work presents a very compact microstrip lowpass-bandpass (LP-BP) triplexer, which is designed and analyzed based on a novel structure. Due to its complex design process, this type of triplexer is rarely designed. Compared to the previous LP-BP triplexers it has the most compact size of 0.006 λ_g^2, whereas an LP-BP triplexer with dimensions smaller than 0.01 λ_g^2 has not been designed yet. This triplexer is designed based on a perfect mathematical method and optimization simultaneously. Its lowpass band has a cut-off frequency of 0.67 GHz, suitable for low-band 5G applications. The resonance frequencies of its bandpass channels are located at 2.15 GHz and 3.19 GHz. These bandpass channels make the proposed triplexer appropriate for 5G mid-band applications. This triplexer can suppress the harmonics from the first up to 8th harmonic. The bandpass channels are flat and wide with two fractional bandwidths (FBW) of 15% and 11.97%. To prove the designing process and its simulation results, the presented novel LP-BP triplexer is fabricated and experimentally measured. The comparison results show that the experimental measurement confirms the simulation results. The close alignment between the measurements and simulation results demonstrates a high level of accuracy of our designing method.

INDEX TERMS Triplexer, microstrip, compact, 5G, insertion loss, lowpass-bandpass.

I. INTRODUCTION

Designing a lowpass-bandpass (LP-BP) triplexer with a compact size, low losses, and low group delay is crucial in RF communication as it enables efficient use of spectrum, reliable signal transmission, and high-speed communication, thereby enhancing overall system performance. In the modern multi-channel communication systems, for mixing or dividing signals we need to handle lowpass and bandpass signals. Hence, various types of microstrip filtering devices have been designed in recent years [1], [2], [3], [4], [5], [6]. Meanwhile, the design of multiplexers [7], [8] and

The associate editor coordinating the review of this manuscript and approving it for publication was Jjun Cheng.

triplexers [9] is more important. Because they are less designed due to their complex design process. The microstrip triplexer is an essential component in RF communication as it allows for the concurrent transmission and reception of multiple signals through a single channel. By enabling simultaneous communication, the triplexer optimizes the use of available bandwidth, allowing for increased data transfer rates and improved overall system performance. This is particularly important in modern wireless communication systems where the demand for high-speed data transmission is continuously growing. The triplexer's ability to separate and combine different frequencies ensures that multiple signals can be transmitted and received simultaneously without interference, resulting in enhanced communication capabilities and improved network efficiency. Until now, the diplexers and triplexers that have lowpass channels have been designed less. Because for designing them, two separate and different lowpass and bandpass resonators must be designed and analyzed. However, in most bandpass devices like diplexers, we only need one type of resonator (but with different dimensions).

Due to the lack of this type of filtering devices, an ultra-compact microstrip LP-BP triplexer with a high performance is designed, fabricated and measured in this work. The lowpass cut-off frequency of this triplexer is located at 670 MHz. It makes this device suitable for low-band 5G applications. The bandpass operating frequencies are 2.15 GHz and 3.19 GHz for the mid-band 5G wireless network, which covers 1-6 GHz. The proposed LP-BP triplexer can suppress harmonics from the 1st harmonic up to the 8th harmonic after its lowpass band.

The paper is organized as follows: First a review of the previous related works has been done in Section II. In Section III, the proposed triplexer is designed and analyzed based on novel mathematical and optimization methods. Then, the simulation and measurement results are presented in Section IV. Also, in this section a perfect comparison between our triplexer and the previous works is done. Finally, the conclusion is presented in the last section.

A. LITERATURE REVIEW

Four microstrip LP-BP (lowpass-bandpass) triplexers have been designed and presented in [9], [10], [11], and [12]. In [9], the patch cells and spiral coupled lines, in [10] a balun-integrated switchable structure, in [11] the stub-loaded hairpin resonators and in [12] the interdigital cells and common lumped-element ripple-resonance resonator are used. These LP-BP triplexers are large, while the introduced structures in [9], [10], and [12], couldn't suppress the harmonics well. The problems of having large sizes and unsuppressed harmonics are remained in the presented microstrip bandpass triplexers in [13], [14], [15], and [16]. The other common problems of these bandpass triplexers are their high insertion losses and narrow channels. Several types of microstrip LP-BP diplexers with large dimensions and unsuppressed harmonics are presented in [17], [18], [19], and [20]. However, the presented diplexers in [17] and [18] have improved insertion losses at their channels. The group delay is an important factor that has not been investigated in some previously reported passive filtering devices [21], [22]. Also, some designed microstrip filtering devices [6], [23], [24], [25], [26] failed to reduce the maximum group delay below 1 ns.

II. PROPOSED TRIPLEXER: STRUCTURE DESIGN AND ANALYSIS

To implement an LP-BP triplexer, its basic structure must include a lowpass filter (LPF) and two bandpass filters (BPFs) with isolated output ports. It is common to use coupled lines in the structure of bandpass resonators. But to design a LPF, a transmission line loaded by the shunt stubs with dominant capacitive characteristics is usually used. Accordingly, we proposed the basic LP-BP triplexer structure as presented in Fig.1. It consists of the transmission lines (TLs) loaded by shunt stubs and coupled lines. The structure of each filter is specified. Each BPF consists of a pair of coupled lines. In addition to the coupled lines, BPF1 includes an open-loop loaded by an internal shunt stub while BPF2 consists of the transmission lines loaded by two stubs. By adding TL8, TL9, TL10, Stub 4, Stub 5 and Stub 6 to the transmission line connected to the common port, we can create a lowpass channel and improve the bandpass resonators. The basic semi-layout of our triplexer with its approximated equivalent LC circuit are presented in Fig.2. The admittances of the Stubs 1-6 are depicted by Y_1-Y_6, respectively. The equivalents of the transmission lines TL1-TL10 are the inductors L_1-L_{10} respectively.

The approximated LC model of the coupled lines with length of $2l_1$ are shown by the coupled capacitors and inductors C and L_1, respectively. The effects of bends are considerable at frequencies higher than 10 GHz [19]. Hence, we could ignore them in the approximated LC circuit. In this approximated model, the inductors L_1 are the equivalents of the T-Lines with the physical lengths l_1. To achieve a more

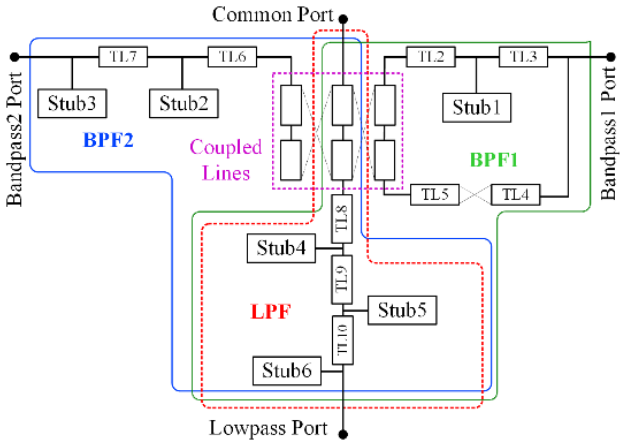

FIGURE 1. General configuration of our LP-BP triplexer.

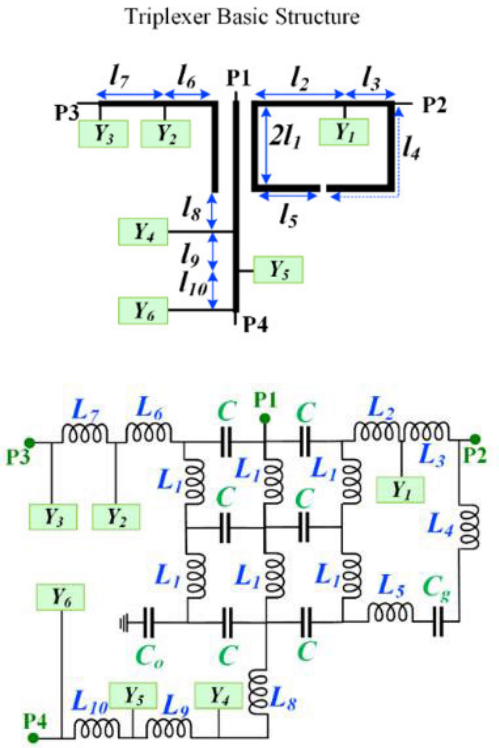

FIGURE 2. Basic semi-layout structure of the proposed triplexer with its approximated equivalent LC circuit.

accurate model of the coupled lines, we have to divide the T-Line (with the physical length $2l_1$) into some smaller lines.

In this case, the number of coupling capacitors can be increased. However, analyzing a more accurate LC model is very difficult mathematically. With the aim of easier calculations to find the behavior of our basic resonators, we analyzed the layout and LC circuits of our LPF and BPFs separately. Fig.3 illustrates the semi-layout and approximated LC circuit of the bandpass resonator 1, where the effect of coupling is presented by C capacitor.

Z_A, Z_B and Z_C are defined in the LC circuit. The terminal ports are depicted by P1 and P2. The *ABCD* transmission

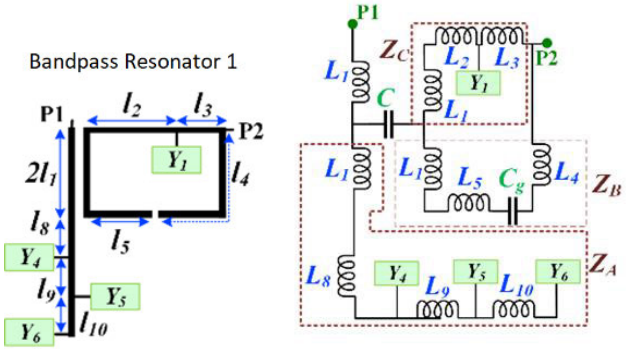

FIGURE 3. The bandpass resonator 1 and its approximated equivalent LC circuit.

matrix of this resonator is calculated as follows:

$$T_{B1} = \begin{bmatrix} A_{B1} & B_{B1} \\ C_{B1} & D_{B1} \end{bmatrix} = \begin{bmatrix} 1 & j\omega L_1 \\ 0 & 1 \end{bmatrix} \times \begin{bmatrix} 1 & 0 \\ \frac{1}{Z_A} & 1 \end{bmatrix} \times \begin{bmatrix} 1 & \frac{1}{j\omega C} + \frac{Z_B Z_C}{Z_B + Z_C} \\ 0 & 1 \end{bmatrix} \quad (1)$$

ω is the angular frequency. After calculation, T_{B1} and Z_A can be obtained by:

$$T_{B1} = \begin{bmatrix} 1 + \frac{j\omega L_1}{Z_A} & \frac{j\omega L_1}{Z_A}(1 + \frac{Z_B Z_C}{Z_B + Z_C}) + \frac{1}{j\omega C} + \frac{L_1}{CZ_A} + \frac{Z_B Z_C}{Z_B + Z_C} \\ \frac{1}{Z_A} & 1 + \frac{1}{j\omega C Z_A} + \frac{Z_B Z_C}{Z_A Z_B + Z_A Z_C} \end{bmatrix} \quad (2)$$

$$Z_A = \frac{1}{\frac{1}{\frac{1}{\frac{1}{Y_6} + j\omega L_{10}} + Y_5} + j\omega L_9} + Y_4 + j\omega L_8 \quad (3)$$

Using the *ABCD* transmission matrix of the bandpass resonator 1, we can calculate the transfer function $H_{B1}(j\omega)$ under the following conditions:

$$H_{B1}(j\omega) = \frac{V_2}{V_1} \rightarrow H_{B1}(j\omega) = \frac{1}{A_{B1}} \; for \; B_{B1} = 0 \quad (4)$$

where, V_1 and V_2 are the voltages of the terminal ports. Substituting A_{B1} and B_{B1} from Equation (2) in Equation (4) results in:

$$H_{B1}(j\omega) = \frac{1}{A_{B1}} = \frac{Z_A}{Z_A + j\omega L_1} \quad (5)$$

$$B_{B1} = 0 \rightarrow \frac{j\omega L_1}{Z_A}(1 + \frac{Z_B Z_C}{Z_B + Z_C}) + \frac{1}{j\omega C} + \frac{L_1}{CZ_A} + \frac{Z_B Z_C}{Z_B + Z_C} = 0 \rightarrow \frac{Z_B Z_C}{Z_B + Z_C} = -\frac{C(Z_A + j\omega L_1) + L_1}{C(Z_A + j\omega L_1)} \quad (6)$$

The coupling capacitor (C) usually has very small value in pF (or fF). Also, our target operating frequency and the inductors are in GHz and nH respectively. Under these conditions, we can use the following approximation:

$$C(Z_A + j\omega L_1) + L_1 \approx L_1 \rightarrow \frac{Z_B Z_C}{Z_B + Z_C} \approx -\frac{L_1}{C(Z_A + j\omega L_1)} \quad (7)$$

For the bandpass resonator 1, the value of the transfer function at the passband will be near 1. Therefore, we can write:

$$H_{B1}(j\omega_1) = \frac{Z_A}{Z_A + j\omega_1 L_1} = 1 \rightarrow Z_A \rangle\rangle j\omega_1 L_1 \rightarrow \frac{1}{\frac{1}{\frac{1}{\frac{1}{Y_6} + j\omega_1 L_{10}} + Y_5} + j\omega_1 L_9} + Y_4 + j\omega_1 L_8 \rangle\rangle j\omega_1 L_1 \quad (8)$$

where ω_1 is the angular operating frequency of the bandpass resonator 1. Equations (7) and (8) show the conditions of working this resonator as a bandpass resonator. According to this, a high degree of freedom exists to adjust the dimensions. However, we have to consider the conditions of the other resonators too. Hence, the semi-layout and corresponding LC circuit (approximated) of the bandpass resonator 2 is presented in Fig.4, where the impedances Z_D and Z_E are marked. The impedance Z_A is the same as presented in Fig.2 and defined in Equation (3).

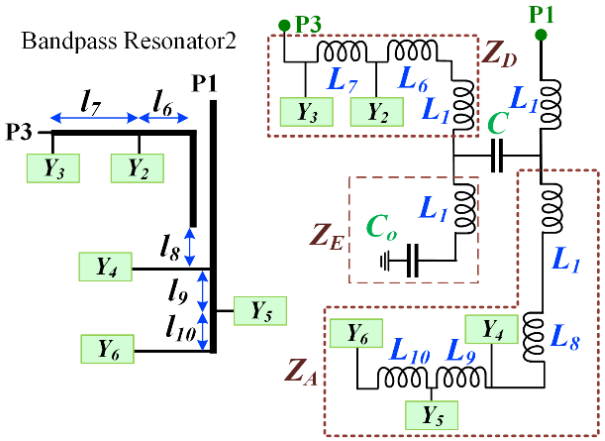

FIGURE 4. The bandpass resonator 2 and its approximated equivalent LC circuit.

The terminal ports of the bandpass resonator 2 are depicted by P1 and P3. The *ABCD* transmission matrix of this resonator is calculated as follows:

$$T_{B2} = \begin{bmatrix} A_{B2} & B_{B2} \\ C_{B2} & D_{B2} \end{bmatrix} = \begin{bmatrix} 1 & j\omega L_1 \\ 0 & 1 \end{bmatrix} \times \begin{bmatrix} 1 & 0 \\ \frac{1}{Z_A} & 1 \end{bmatrix} \times \begin{bmatrix} 1 & \frac{1}{j\omega C} \\ 0 & 1 \end{bmatrix} \times \begin{bmatrix} 1 & 0 \\ \frac{1}{Z_E} & 1 \end{bmatrix} \times \begin{bmatrix} 1 & Z_D \\ 0 & 1 \end{bmatrix} \tag{9}$$

After calculation, T_{B2} and Z_E can be given by:

$$T_{B2} = \begin{bmatrix} a & b \\ c & d \end{bmatrix} \tag{10}$$

where:

$$a = 1 + \frac{j\omega L_1}{Z_A} + \frac{1}{Z_E}[j\omega L_1 + \frac{1}{j\omega C}(1 + \frac{j\omega L_1}{Z_A})] \tag{11}$$

$$b = (1 + \frac{j\omega L_1}{Z_A})Z_D + [j\omega L_1 + \frac{1}{j\omega C}(1 + \frac{j\omega L_1}{Z_A})](\frac{Z_D}{Z_E} + 1) \tag{12}$$

$$c = \frac{1}{Z_A} + \frac{1}{Z_E}(1 + \frac{1}{jZ_A\omega C}) \tag{13}$$

$$d = \frac{Z_D}{Z_A} + (1 + \frac{1}{jZ_A\omega C})(\frac{Z_D}{Z_E} + 1) \tag{14}$$

$$Z_E = \frac{1}{j\omega C_O} + j\omega L_1 \tag{15}$$

The coupling capacitor (C) is usually very small in pF (or fF). Similar to the bandpass resonator 1, our target operating frequency and the inductors are in GHz and nH respectively. for a small coupling capacitor, we can use the following approximations:

$$1 + \frac{j\omega L_1}{Z_A} + \frac{1}{Z_E}[j\omega L_1 + \frac{1}{j\omega C}(1 + \frac{j\omega L_1}{Z_A})] \approx \frac{1}{j\omega C Z_E}(1 + \frac{j\omega L_1}{Z_A}) \tag{16}$$

$$(1 + \frac{j\omega L_1}{Z_A})Z_D + [j\omega L_1 + \frac{1}{j\omega C}(1 + \frac{j\omega L_1}{Z_A})](\frac{Z_D}{Z_E} + 1) \approx \frac{1}{j\omega C}(1 + \frac{j\omega L_1}{Z_A})(\frac{Z_D}{Z_E} + 1) \tag{17}$$

$$\frac{1}{Z_A} + \frac{1}{Z_E}(1 + \frac{1}{jZ_A\omega C}) \approx \frac{1}{jZ_AZ_E\omega C} \tag{18}$$

$$\frac{Z_D}{Z_A} + (1 + \frac{1}{jZ_A\omega C})(\frac{Z_D}{Z_E} + 1) \approx \frac{1}{jZ_A\omega C}(\frac{Z_D}{Z_E} + 1) \tag{19}$$

By applying these approximations in Equation (10), the following result can be obtained:

$$T_{B2} = \begin{bmatrix} A_{B2} & B_{B2} \\ C_{B2} & D_{B2} \end{bmatrix} = \begin{bmatrix} \frac{1}{j\omega Z_E C}(1 + \frac{j\omega L_1}{Z_A}) & \frac{1}{j\omega C}(1 + \frac{j\omega L_1}{Z_A})(\frac{Z_D}{Z_E} + 1) \\ \frac{1}{jZ_EZ_A\omega C} & \frac{1}{jZ_A\omega C}(\frac{Z_D}{Z_E} + 1) \end{bmatrix} \tag{20}$$

Using the *ABCD* transmission matrix of the bandpass resonator 2, we can calculate its transfer function $H_{B2}(j\omega)$ under the following conditions:

$$H_{B2}(j\omega_2) = \frac{V_3}{V_1} \rightarrow H_{B2}(j\omega_2) = \frac{1}{A_{B2}} \; for \; B_{B2} = 0 \tag{21}$$

where, V_1 and V_3 are the voltages at the terminals P1 and P3, respectively. Substituting Equation (20) in Equation (21) for B_{B2} =0 results in:

$$B_{B2} = 0 \rightarrow (1 + \frac{j\omega_2 L_1}{Z_A})(\frac{Z_D}{Z_E} + 1) = 0 \rightarrow Z_D = -Z_E \tag{22}$$

For the bandpass resonator 2, the value of the transfer function at its passband must be near 1. Therefore, we can write that:

$$|H_{B2}(j\omega)| = 1 \rightarrow \left|\frac{j\omega Z_AZ_EC}{Z_A + j\omega_2 L_1}\right| = 1 \rightarrow \begin{cases} Z_A \rangle\rangle j\omega_2 L_1 \\ and \\ \omega_2 Z_AZ_EC = 1 \rightarrow \omega_2 = \frac{1}{Z_AZ_EC} \end{cases} \tag{23}$$

where ω_2 is the angular operating frequency of the bandpass resonator 2. Equations (22) and (23) show the conditions of working the resonator 2 as a bandpass resonator.

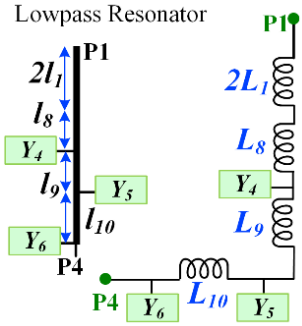

FIGURE 5. The lowpass resonator and its approximated equivalent LC circuit.

The semi-layout and its corresponding LC circuit of the lowpass resonator is shown in Fig. 5.

The ABCD matrix of the lowpass resonator is extracted from its LC model as follows:

$$T_L = \begin{bmatrix} A_L & B_L \\ C_L & D_L \end{bmatrix} = \begin{bmatrix} 1 & j\omega(2L_1+L_8) \\ 0 & 1 \end{bmatrix} \times \begin{bmatrix} 1 & 0 \\ Y_4 & 1 \end{bmatrix} \times \begin{bmatrix} 1 & j\omega L_9 \\ 0 & 1 \end{bmatrix} \times \begin{bmatrix} 1 & 0 \\ Y_5 & 1 \end{bmatrix} \times \begin{bmatrix} 1 & j\omega L_{10} \\ 0 & 1 \end{bmatrix} \times \begin{bmatrix} 1 & 0 \\ Y_6 & 1 \end{bmatrix} \quad (24)$$

After calculations, the values of A_L and B_L are obtained as follows:

$$A_L = [(1 + j\omega(2L_1+L_8)Y_4)(1 + j\omega L_9 Y_5) + j\omega Y_5(2L_1+L_8)][1 + j\omega L_{10}Y_6] + Y_6[j\omega(2L_1+L_8) + j\omega L_9 - \omega^2(2L_1+L_8)Y_4 L_9] \quad (25)$$

$$B_L = [(1 + j\omega(2L_1+L_8)Y_4)(1 + j\omega L_9 Y_5) + j\omega Y_5(2L_1+L_8)]j\omega L_{10} + j\omega(2L_1+L_8) + j\omega L_9 - \omega^2(2L_1+L_8)Y_4 L_9 \quad (26)$$

The transfer function of the lowpass resonator can be calculated using Equations (24), (25) and (26) as follows:

$$H_L(j\omega) = \frac{V_4}{V_1} \rightarrow H_{B2}(j\omega) = \frac{1}{A_L} \; for \; B_L = 0 \quad (27)$$

where V_1 and V_4 are the voltages at P1 and P4 terminals, respectively. At an angular -3dB cut-off frequency of ω_c we can calculate $H_L(j\omega)$ as:

$$G_L = 20\log(H_L(j\omega_C)) = -3dB \rightarrow H_L(j\omega_C) \approx 0.7 \rightarrow A_L = 1.42 \;\&\; B_L = 0 \quad (28)$$

Applying the first condition A_L =1.42 results in (29), as shown at the bottom of the page, where ω_{C1} is the lowpass resonator cut-off frequency. Applying B_L =0 leads to (30), as shown at the bottom of the page, where ω_{C2} is another cut-off frequency of our lowpass resonator. Since our lowpass resonator has only a cut-off frequency we allow:

$$\omega_{C1} = \omega_{C2} \rightarrow L_{10}Y_6 + (Y_5+Y_6)L_9 + (Y_5+Y_4+Y_6)(L_8+2L_1) = Y_6(L_{10} + L_8Y_4L_{10} + 2L_1 + L_8 + L_9) \quad (31)$$

By applying Equation (31), we can obtain a lowpass resonator. As can be seen from the above equations, a high degree of freedom exists to tune the dimensions. Accordingly, we can easily miniaturize the dimensions of the lowpass

$$A_L = 1.42 \rightarrow -\omega_C^2(L_9Y_5L_{10}Y_6 + 2L_1Y_4L_{10}Y_6 + 2L_1Y_4L_9Y_5 + Y_4L_8L_{10}Y_6 + Y_4L_8L_9Y_5 + Y_4L_9Y_6L_8 + Y_5L_8L_{10}Y_6 + 2L_1Y_5L_{10}Y_6 + 2Y_4L_9L_1Y_6) + j\omega_C(L_{10}Y_6 + (Y_5+Y_6)L_9 + (Y_5+Y_4+Y_6)L_8 + 2L_1(Y_4+Y_5+Y_6) - Y_4Y_5Y_6L_9L_{10}\omega_C^2(2L_1+L_8)) = 0.42 \rightarrow$$

$$\begin{cases} L_{10}Y_6 + (Y_5+Y_6)L_9 + (Y_5+Y_4+Y_6)L_8 + 2L_1(Y_4+Y_5+Y_6) - \omega_C^2 Y_4Y_5Y_6L_9L_{10}(2L_1+L_8) = 0 \\ -\omega_C^2(L_9Y_5L_{10}Y_6 + 2L_1Y_4L_{10}Y_6 \\ +2L_1Y_4L_9Y_5 + Y_4L_8L_{10}Y_6 + Y_4L_8L_9Y_5 + Y_4L_9Y_6L_8 + Y_5L_8L_{10}Y_6 + 2L_1Y_5L_{10}Y_6 + 2Y_4L_9L_1Y_6) = 0.42 \rightarrow \end{cases}$$

$$\omega_{C1} = \sqrt{\frac{L_{10}Y_6 + (Y_5+Y_6)L_9 + (Y_5+Y_4+Y_6)L_8 + 2L_1(Y_4+Y_5+Y_6)}{Y_4Y_5Y_6L_9L_{10}(2L_1+L_8)}} \quad (29)$$

$$B_L = 0 \rightarrow j\omega_C(L_{10} + L_8Y_4L_{10} + 2L_1 + L_8 + L_9 - \omega_C^2 2L_1Y_4L_9Y_5L_{10} - \omega_C^2 L_9Y_5L_8Y_4L_{10}) - \omega_C^2(L_9Y_5L_{10} + 2L_1Y_4L_{10} + 2L_1Y_4L_9 + L_8Y_4L_9 - 2L_1Y_5L_{10} - Y_5L_8L_{10}) = 0 \rightarrow$$

$$\begin{cases} L_{10} + L_8Y_4L_{10} + 2L_1 + L_8 + L_9 - \omega_C^2(2L_1Y_4L_9Y_5L_{10} + L_9Y_5L_8Y_4L_{10}) = 0 \\ and \\ 2L_1(Y_4L_{10} + Y_4L_9 - Y_5L_{10}) + L_8Y_4L_9 + L_9Y_5L_{10} - Y_5L_8L_{10} = 0 \end{cases} \rightarrow$$

$$\omega_{C2} = \sqrt{\frac{L_{10} + L_8Y_4L_{10} + 2L_1 + L_8 + L_9}{Y_4Y_5L_9L_{10}(2L_1+L_8)}} \quad (30)$$

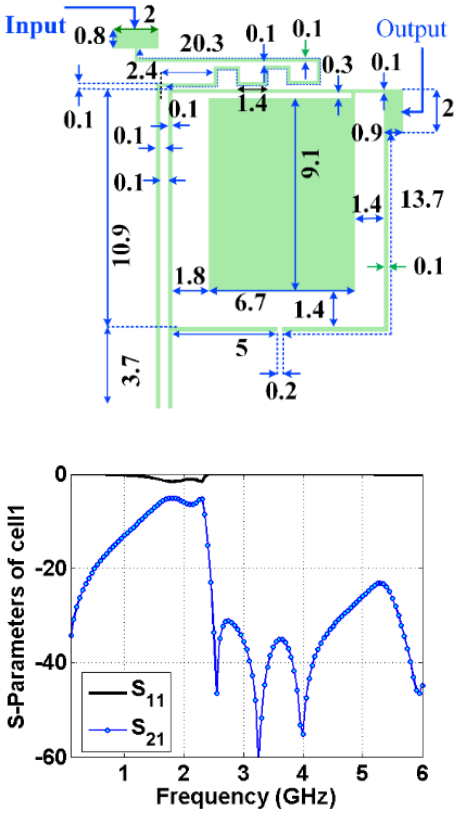

FIGURE 6. Proposed microstrip cell1 (frequency response and basic layout).

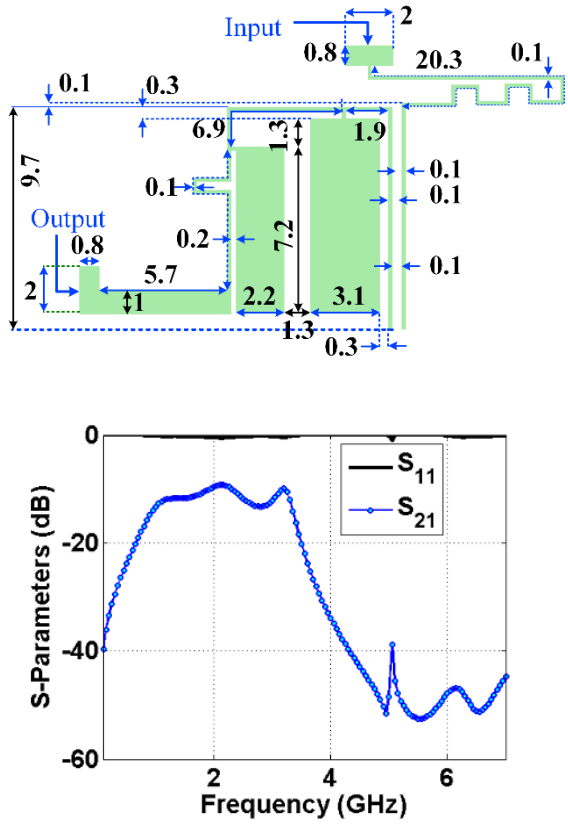

FIGURE 7. Proposed microstrip cell2 (frequency response and basic layout).

resonator based on Equation (31). The layouts and frequency responses of the bandpass cells (named cell1 and cell2) are presented in Figs.6 and 7, respectively. These cells are obtained based on the bandpass resonators 1 and 2 and their mathematical analysis. The shunt stubs are presented by the rectangular patch cells. All thin T-lines have 0.1 mm wide. The dimensions of the terminal ports are tuned for being 50Ω. All simulation results are extracted using ADS software (EM simulator) by small linear steps. We used Rogers RT/Duroid5880 substrate to design and simulation of the proposed triplexer. Our used substrate has a loss tangent of 0.0009, a dielectric constant of 2.22 and h=31 mil. Some other microstrip sections are added to improve the frequency responses of cells 1 and 2.

In Figure 3, if we set $Z_A = j\omega L_1$, the approximated equivalent model of microstrip cell1 can be obtained. Because by removing the stubs with admittances y_4, y_5 and y_6 and physical lengths l_8, l_9, l_{10} in bandpass resonator 1, the approximated model of cell1 can be obtained. Under this condition and using T_{B1}, we can calculate S_{21} of this cell as follows:

$$S_{21} = \frac{2}{A_{B1} + B_{B1}/Z_0 + Z_0 C_{B1} + D_{B1}} \rightarrow$$
$$S_{21} \approx \frac{2}{2 + \frac{2}{j\omega C Z_0} + \frac{Z_0}{j\omega L_1} - \frac{1}{\omega^2 C L_1}} \tag{32}$$

where Z_0 is the impedance of terminals. Moreover, the coupling capacitor is assumed to be very small. When -20log $|S_{21}|$ has a large negative value, we have transmission zeros (TZs). Therefore, the TZs can be obtained at the angular frequency ω_z under the following condition:

$$2 + \frac{2}{j\omega_z C Z_0} + \frac{Z_0}{j\omega_z L_1} - \frac{1}{\omega_z^2 C L_1} \approx 0 \rightarrow$$
$$\begin{cases} \frac{1}{\omega_z^2 C L_1} = 2 \rightarrow \omega_z = \sqrt{\frac{1}{2CL_1}} \\ \frac{2}{j\omega_z C Z_0} + \frac{Z_0}{j\omega_z L_1} = 0 \end{cases} \tag{33}$$

Equation (33) shows only one TZ created by the coupled lines but the simulation results show three TZs of cell1 created by the internal stub and the thin T-line connected to the input port. This is due to the approximations we used in our mathematical analysis. As we mentioned before, we used some approximations to analyze the proposed structures because it is very difficult to analyze a more accurate LC model mathematically. For example, to easy calculations the effect of the thin T-line is not considered, we used an approximated LC model of the coupled lines and we ignored the effects of bends in the approximated LC circuit.

Fig.8 shows the BPF1, which is designed based on the analyzed bandpass resonator1. BPF1 is the upgraded version

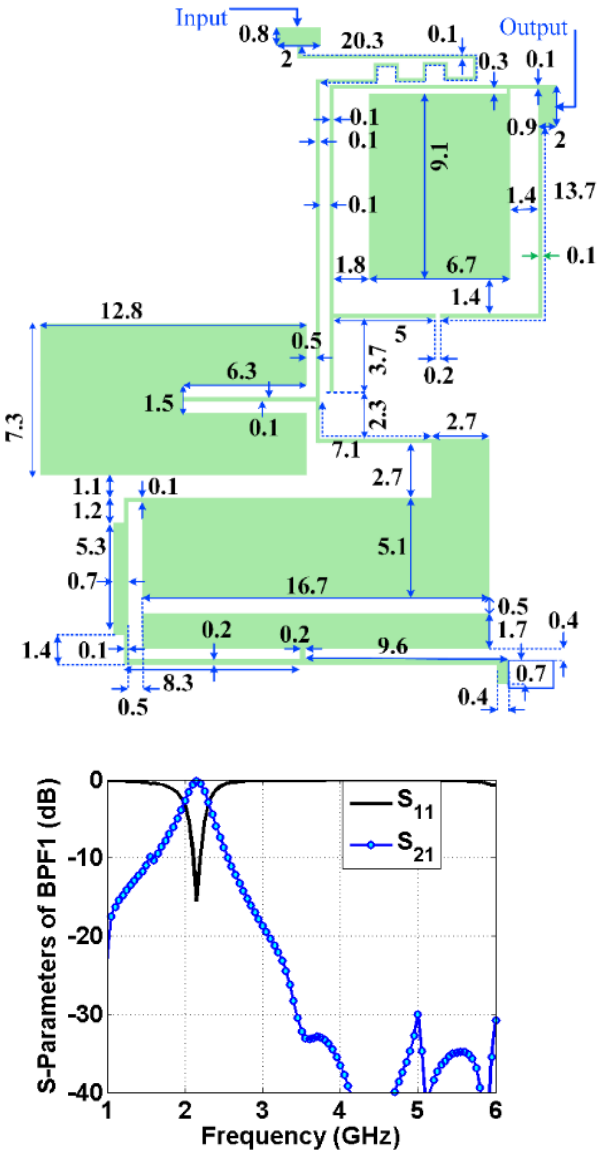

FIGURE 8. Proposed BPF1: frequency response and layout.

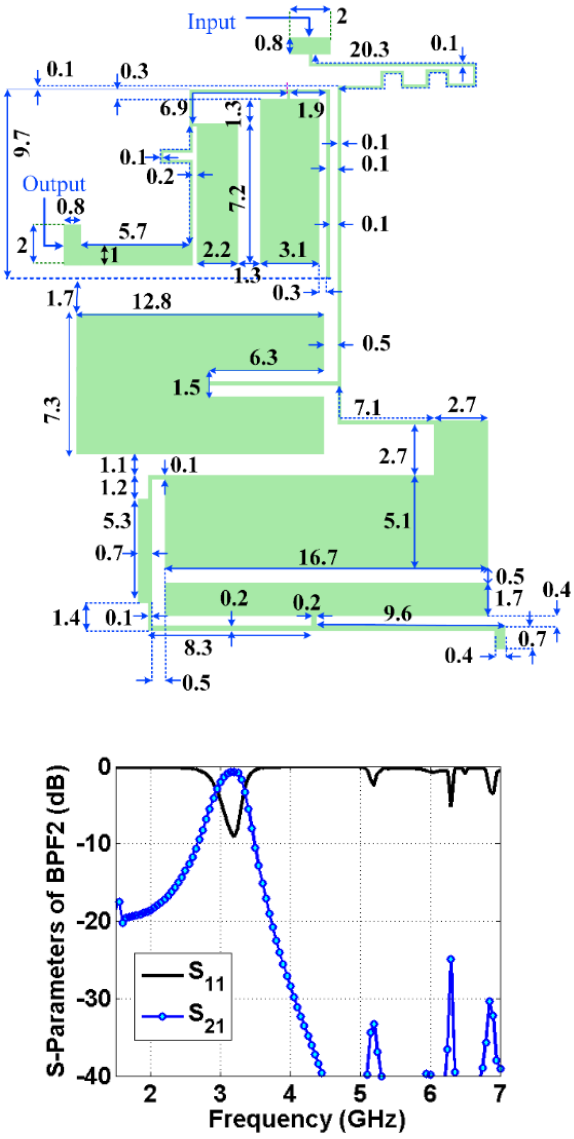

FIGURE 9. Proposed BPF2: frequency response and layout.

of the cell1. Fig.8, includes the layout and frequency response of this filter. As presented, the values of insertion and return losses are improved. The harmonics of this structure are suppressed up to 6 GHz. The frequency response and the layout configuration of the BPF2 are presented in Fig.9. This filter is the upgraded version of the microstrip cell2. It is designed based on the analyzed bandpass resonator 2. It can attenuate the harmonics up to 7 GHz. The open loop structure is used in the upper part of BPF1 so that its frequency response is shifted to the left compared to BPF2. Therefore, BPF1 and BPF2 suppress the harmonics up to 6 GHz and 7 GHz, respectively.

Fig.10 shows the proposed LPF, which is designed based on the analyzed lowpass resonator. However, to improve the frequency response we optimized this structure. Similar to the other filters, it is simulated by ADS software using the small steps of the EM simulator.

By integrating the BPF1, BPF2 and LPF our LP-BP triplexer is obtained as shown in Fig.11, where all dimensions are in mm. The overall size of this triplexer (including the 50 Ω microstrip cells that are connected to the SMA connectors) is only $0.091\lambda g \times 0.072\lambda g$ (31.4mm×25mm). In the main body of our triplexer, the dimensions of the proposed filters are not changed. To show how we could optimize the frequency response, the effect of changing some important lengths and widths is depicted in Fig.12. As depicted, changing l_a has direct effects on the middle and last channels. Meanwhile, by tuning l_a (the physical length of coupled lines) we can reduce the return loss in the bandpass channels.

Excessive increase and decrease of l_b will destroy the last passband, so that l_b =6.9 mm is a suitable value. Similarly, an excessive increase of l_c can increase the insertion loss at the last passband. As illustrated, decreasing w_a increases the

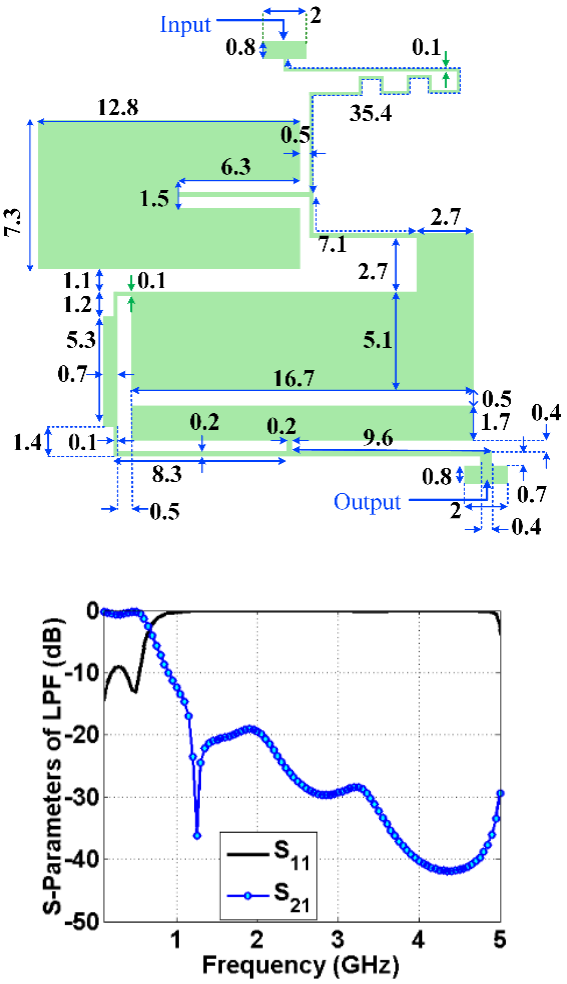

FIGURE 10. Layout and frequency response of the proposed LPF (unit: mm).

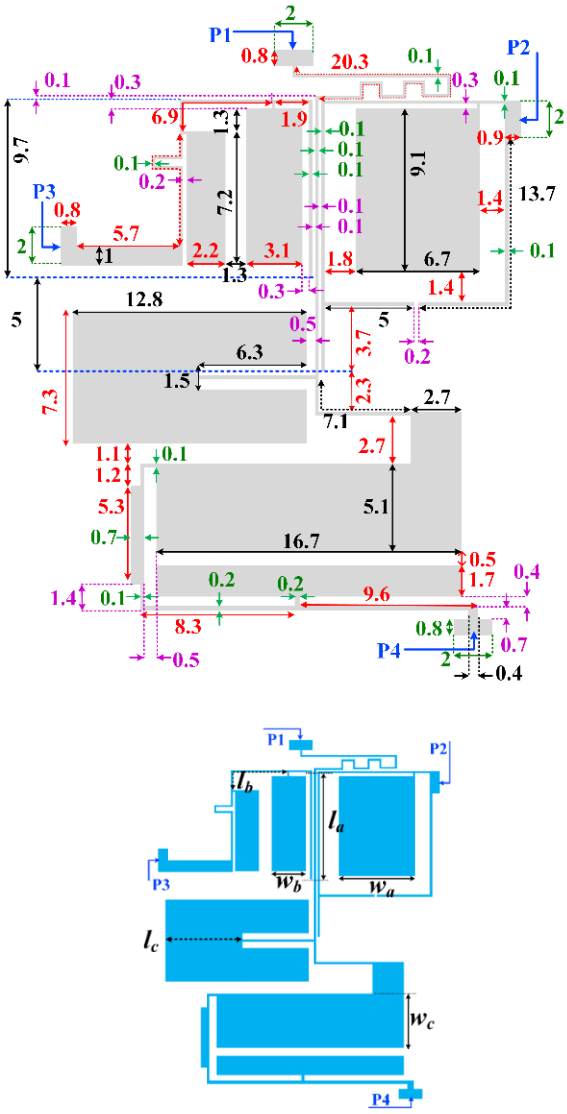

FIGURE 11. Final layout configuration of the proposed triplexer (unit: mm).

return loss inside the middle channel. Therefore, w_a =6.7 mm is an appropriate value. Since, the shunt stub with a physical width of w_b is related to the bandpass section II (the last channel), excessive increase and decrease of w_b will destroy the last passband. As shown in Fig.12, by tuning w_c we can control the lowpass channel and the last channel simultaneously. Meanwhile, increasing this width can suppress the harmonics significantly.

A. RESULTS AND COMPARISON

Both simulated and measurement results are obtained using ADS software and an HP8757A network analyzer, respectively. The close agreement between the two sets of results is worth noting. However, it is important to acknowledge that the measured losses are slightly higher than the simulated losses due to SMA losses. The ADS software, a widely used tool for circuit design and analysis, is employed to simulate the performance of the proposed triplexer. This software allows for accurate modeling of the resonator's behavior and provides valuable insights into its characteristics. On the other hand, the HP8757A network analyzer, a highly reliable instrument for measuring the performance of RF and microwave devices, is utilized to obtain the actual measurements of the proposed triplexer. The fact that both the simulated and measured results are in close agreement suggests that the design and analysis of the proposed triplexer are successful. However, it is worth mentioning that the measured losses are slightly higher than the simulated losses. This discrepancy can be attributed to SMA losses. These losses can affect the overall performance of the resonators and result in slightly higher measured losses compared to the simulations. Fig.13, shows the simulated and measured scattering parameters from 0.1 GHz to 6.4 GHz. As shown in this figure, the cut-off frequency of the first channel is located at 0.67 GHz, which is suitable for 5G low-band applications. The second channel is from 1.985 GHz to 2.305 GHz, where

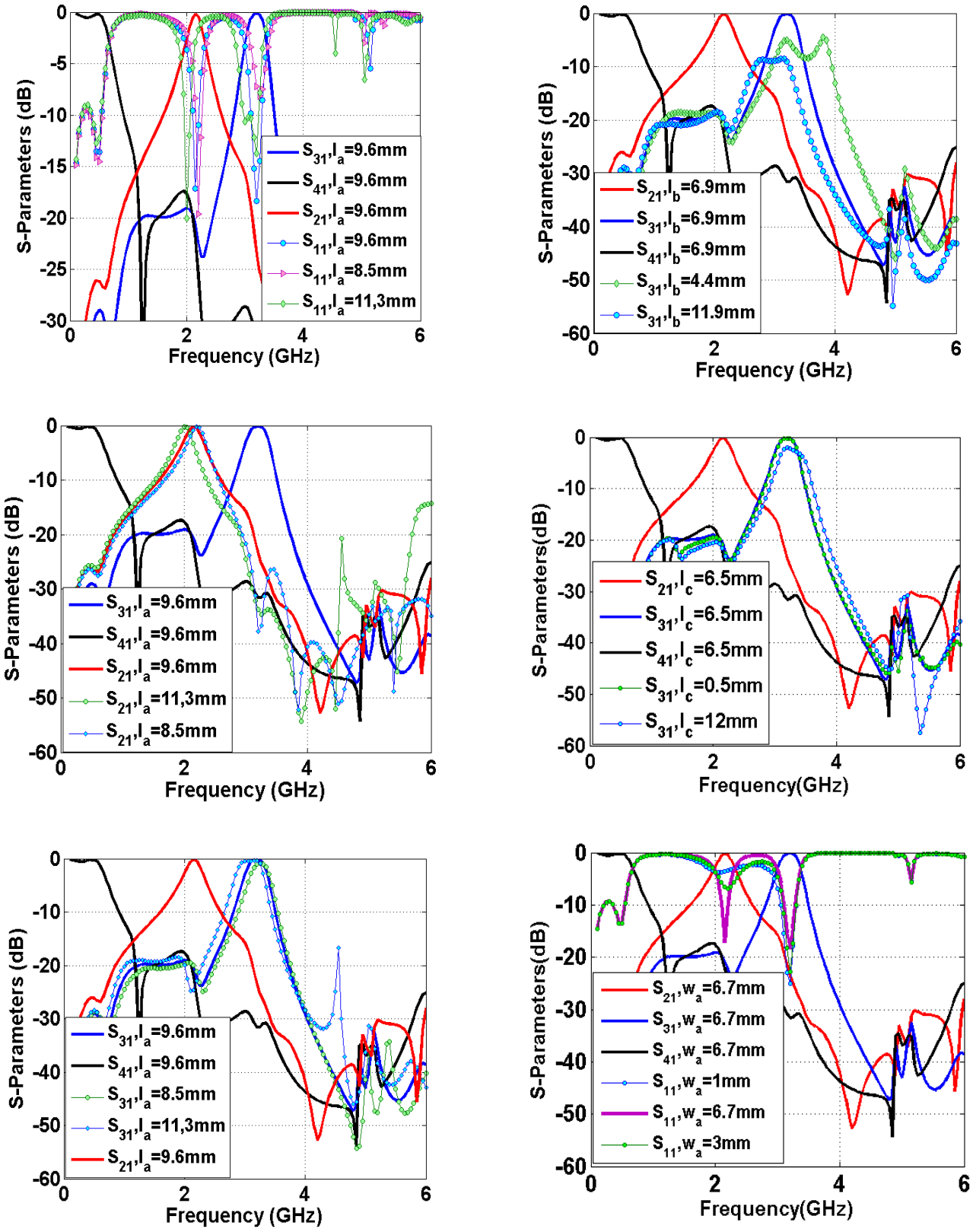

FIGURE 12. The effects of some significant lengths and widths on the frequency response.

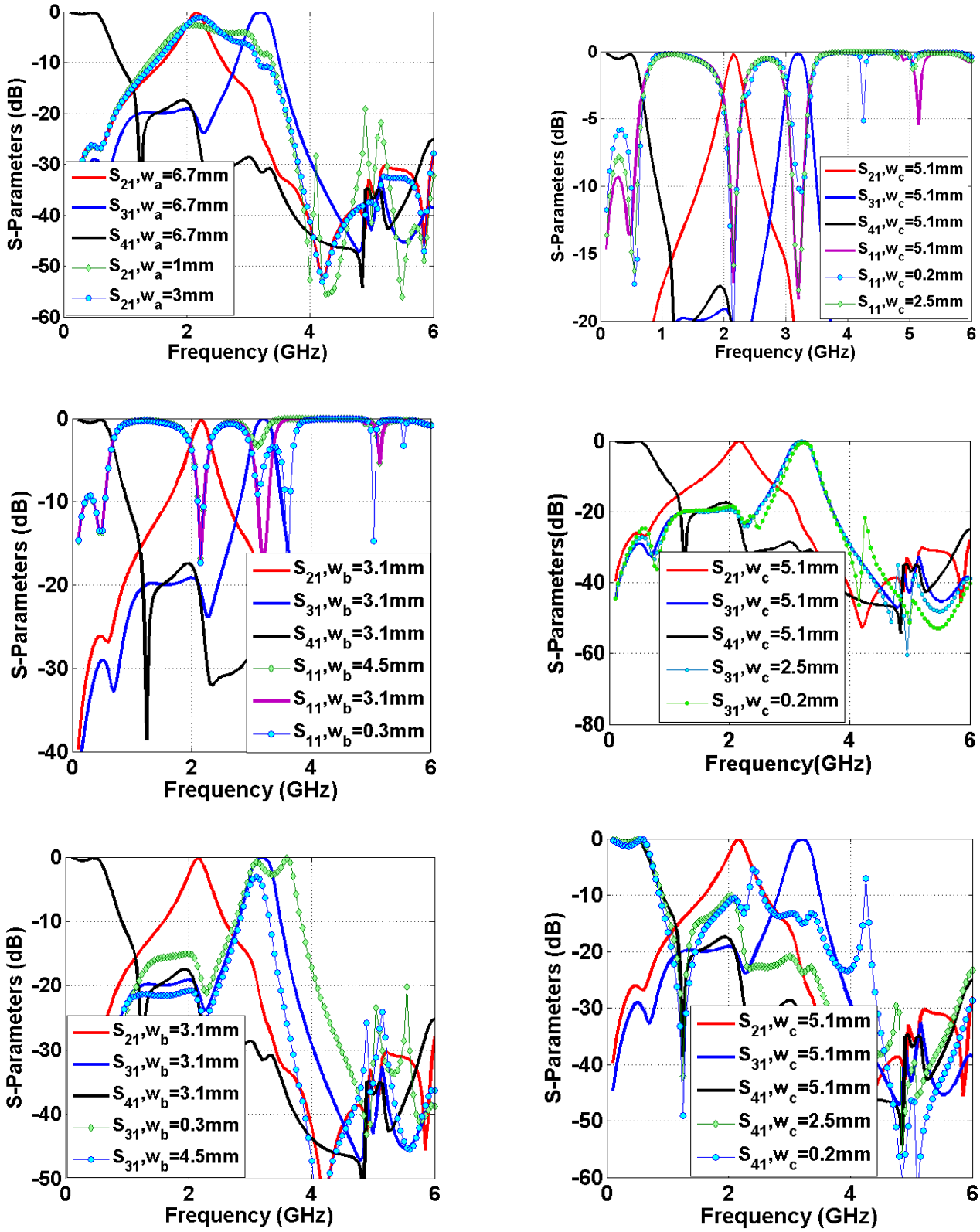

FIGURE 12. *(Continued.)* **The effects of some significant lengths and widths on the frequency response.**

TABLE 1. Frequency response and size of the proposed triplexer in comparison with the previous works.

Refs.	f_{o1}, f_{o2}, f_{o3} (GHz)	IL_1, IL_2, IL_3 (dB)	$\Delta_1, \Delta_2, \Delta_3$ (%)	Size (λ_g^2)	N^{th} SH	I_{Min}	Type
This Triplexer	0.67, 2.15, 3.19	0.55, 0.17, 0.17	15 , 11.97	0.006	8th	-20.5	Lowpass-Bandpass Triplexer
[9]	1.8, 3.2, 6.6	0.54, 0.16, 0.55	15, 8.3	0.021	3rd	-19	Lowpass-Bandpass Triplexer
[10]	0.85, 1.6, 2.1	0.72, 1.66, 1.7	13.9, 12.7	0.048	2nd	-20	Lowpass-Bandpass Triplexer
[11]	1, 2.4, 5.8	0.8, 2.1, 2.5	10, 7	---	6th	-40	Lowpass-Bandpass Triplexer
[12]	0.95, 1.58, 2.8	0.3, 1.16, 2.04	17, 8.1	0.018	3rd	-27	Lowpass-Bandpass Triplexer
[13]	2.3, 3.2, 3.6	0.78, 1.1, 0.62	5.2,5.5,1.6	0.095	No	-14.8	Bandpass Triplexer
[14]	2.67, 3.1, 3.43	0.72, 0.63, 0.71	5.2,2.8,9.4	0.137	No	-20	Bandpass Triplexer
[15]	1, 1.25, 1.5	2.7, 1.8, 3.2	9.5,4.2,4.5	0.064	2nd	-30	Bandpass Triplexer
[16]	1.8 , 3.2, 4.4	1.97, 1.99, 2.3	7.4,7.4,6.2	---	3rd	-20	Bandpass Triplexer
[17]	1.65, 2.57	0.047, 0.16	14	0.037	1st	-21.2	Lowpass-Bandpass Diplexer
[18]	1.88, 3.56	0.12, 0.1	23.8	0.03	3rd	-26	Lowpass-Bandpass Diplexer
[20]	1.46, 2.42	0.68, 0.95	11.13	0.037	4th	-28	Lowpass-Bandpass Diplexer
[21]	2, 3.5	0.3, 1.28	5.5	0.093	2nd	-40	Lowpass-Bandpass Diplexer

f_o: Operating Frequency; IL: Insertion Loss; Δ: Fractional Bandwidth; N^{th} SH: N^{th} Suppressed Harmonic and I_{Min}: Isolation between channels.

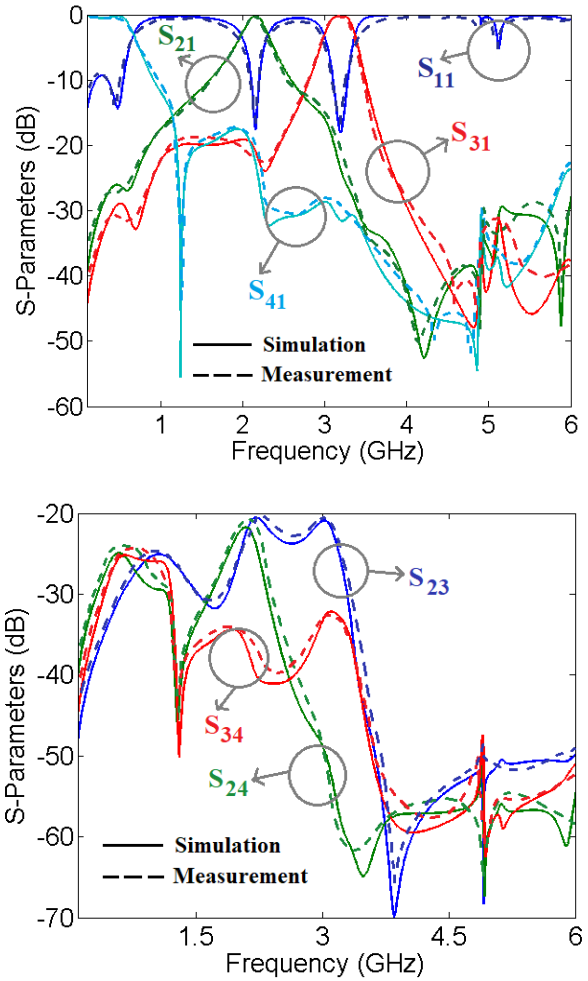

FIGURE 13. Scattering parameters of the designed triplexer (simulation and measurement results).

it operates at 2.155 GHz. The third channel is from 2.990 GHz to 3.37 GHz, which resonates at 3.195 GHz. In this regard, the bandpass channels make our triplexer suitable for 5G mid-band applications. The second and third channels provide two fractional bandwidths (FBW) of 15% and 11.97% respectively. The common port return losses at the low, middle and high channels are approximately 14.2 dB, 17.6 dB and 18.08 dB respectively. As depicted, the triplexer has a good stopband response so that after the lowpass channel all harmonics are suppressed up to 6.4 GHz. Good insertion losses of 0.55 dB, 0.17 dB, and 0.17 dB are archived at the 1st, 2nd, and 3rd bands respectively. As shown in Fig.13, the isolations between the output ports (S_{34}, S_{24} and S_{23}) are better than -20.5 dB. To demonstrate the superiority of our triplexer, we compared it with the previous works and listed the comparison results in Table 1. In this Table, indexes 1-3 are related to the first-third channels respectively. Because the number of LP-BP triplexers is limited, we had to present the other similar microstrip filtering devices in the comparison Table. The size of our triplexer is the most compact, so that it is 67% smaller than the smallest device presented in [12]. In addition to the most compact size, our triplexer has the best harmonic suppression. Because it can attenuate harmonics from the 1st to the 8th harmonics. Meanwhile, none of the references in Table 1 could suppress the 7th harmonic. The other benefits of this triplexer are its low insertion losses and wide FBWs. Improving the isolation in triplexers is more difficult than diplexers. Because for a triplexer, we have to control the isolations of three channels. On the other hand, it is difficult to have a good isolation when the channels are close together. The presented lowpass-bandpass triplexers in [11] and [12] have good isolations better than ours. However, overall, our triplexer outperforms them in terms of size, insertion loss, and suppressed harmonics.

Group delay is an important parameter in all filtering devices such as microstrip triplexers. But unfortunately, many designers neglect to consider and improve it in their designs. Fig.14 shows the group delays of S_{21}, S_{31} and S_{41}, which cover the 2nd, 3rd and 1st channels respectively.

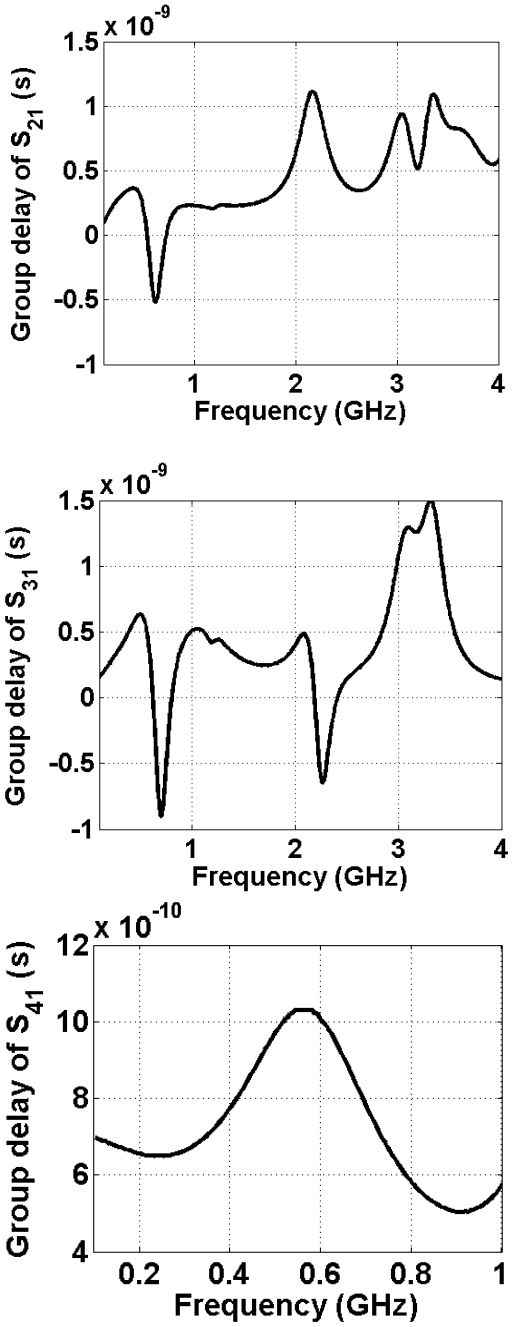

FIGURE 14. Group delays of the designed triplexer.

The results show that the group delay at the 1st, 2nd and 3rd channels are lower than 1 ns, 1.1 ns and 1.5 ns respectively. Table 2 shows the group delay comparison between this work and the previous works. As can be seen, only the triplexer in [9] could improve the group delays better than us. However, our triplexer has the most compact size, better harmonic suppression and wider the last channel. The compact size of the proposed triplexer ensures that it can be easily integrated into various communication systems without occupying excessive

TABLE 2. The maximum group delays of this triplexer and the previous works.

Refs.	Type	Maximum Group Delays at Each Channel
This Triplexer	LP-BP Triplexer	1 ns, 1.1 ns, 1.5 ns
[6]	Bandpass-Bandpass Diplexer	Near 4 ns for both channels
[9]	LP-BP Triplexer	0.79 ns, 0.98 ns, 0.85 ns
[11]	LP-BP Triplexer	1.5 ns, 6 ns, 4.4 ns
[17]	LP-BP Diplexer	1.43 ns, 1.68 ns
[18]	LP-BP Diplexer	2 ns, 1.24 ns
[23]	Tri-Channel Bandpass Filter	Better than 8 ns at all channels
[24]	Bandpass-Bandpass Diplexer	3.15 ns, 2.98 ns
[25]	Quad-Channel Bandpass Filters	9 ns, 6 ns, 6 ns, 5 ns
[26]	Coupler	1.9 ns, 2.3 ns

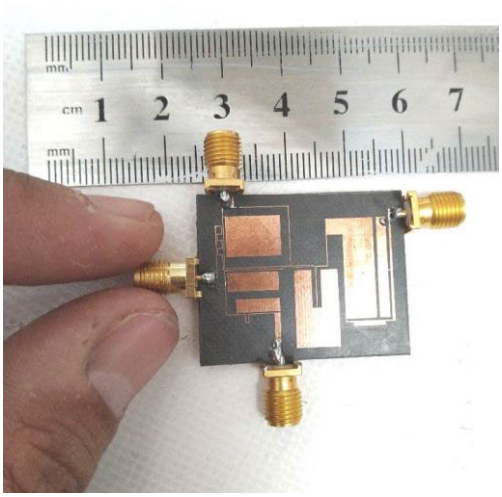

FIGURE 15. The fabricated triplexer.

space. Its novel structure allows for optimized signal separation and combination, resulting in improved communication capabilities and network efficiency. Additionally, the low losses of this triplexer minimize signal degradation, ensuring reliable and high-quality transmission and reception. Furthermore, its wide FBWs enable increased data transfer rates, addressing the growing demand for high-speed communication in modern wireless systems. Fig.15 shows a photograph of the fabricated LP-BP triplexer.

Figure 16 depicts a flowchart of the main idea of obtaining this triplexer. First, a new basic structure of our triplexer is presented. It consists of two BPFs and one LPF. An approximated LC circuit of this basic triplexer is proposed and mathematically analyzed to identify the behavior of the basic structure and easy optimization. Then, the proposed structure is optimized to improve its performance. Finally, the

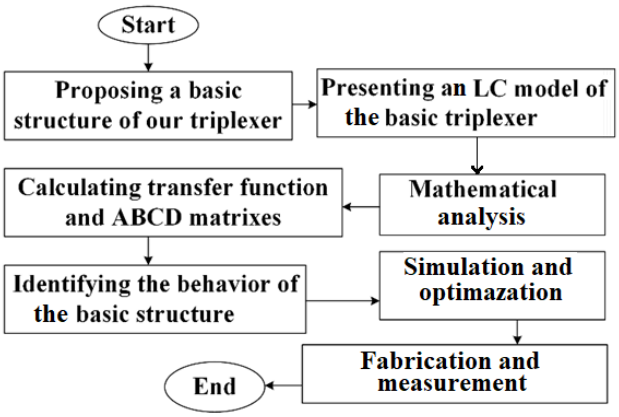

FIGURE 16. A flowchart of the main idea of obtaining the proposed triplexer.

final triplexer is fabricated, measured and compared with the previous works.

III. CONCLUSION

The development of a microstrip triplexer with a compact size, novel structure, low losses, and wide bandwidth is a significant advancement in RF communication technology. This paper has highlighted the importance of such a triplexer in enabling concurrent transmission and reception of multiple signals through a single channel, thereby enhancing the efficiency and utilization of the limited frequency spectrum. We designed, fabricated and measured a microstrip LP-BP (lowpass-bandpass) triplexer based on a novel layout configuration. It includes a novel lowpass filter (LPF) and two optimized bandpass filters (BPFs) which are analyzed mathematically. The final layout is optimized to improve the performance and miniaturization simultaneously. The size of this LP-BP triplexer is only 0.006 λg^2. In addition to having a compact size, the proposed LP-BP has a high performance. This triplexer has low insertion losses, suppressed harmonics, flat channels and wide fractional bandwidths (FBW). The cut-off frequency of its lowpass channel and the resonance frequencies of its bandpass channels can be used for the low-band and mid-band 5G applications, respectively. This triplexer can suppress the harmonics from the 1st up to the 8th harmonics. The bandpass channels are flat and wide with two FBW of 15% and 11.97%. To confirm the simulation results, we fabricated and experimentally measured the designed triplexer.

REFERENCES

[1] D. K. Choudhary, N. Mishra, P. K. Singh, and A. Sharma, "Miniaturized power divider with triple-band filtering response using coupled line," *IEEE Access*, vol. 11, pp. 27602–27608, 2023.

[2] M. Nouri, A. Jafarieh, H. Behroozi, N. K. Mallat, A. Iqbal, M. J. Piran, and D. Lee, "A compact filter and dipole antenna with its phased array filtenna and ADMM-BO learning for use-case analog/hybrid beamforming in 5G mmWave communications," *IEEE Access*, vol. 11, pp. 55990–56007, 2023.

[3] M. Jamshidi, S. I. Yahya, L. Nouri, H. Hashemi-Dezaki, A. Rezaei, and M. A. Chaudhary, "A high-efficiency diplexer for sustainable 5G-enabled IoT in metaverse transportation system and smart grids," *Symmetry*, vol. 15, no. 4, p. 821, Mar. 2023.

[4] M. D. Fadaee, F. Shama, M. S. Feali, and M. S. Gilan, "A miniaturized wide stopband low-pass filter using T and modified L shapes resonators," *ARO-Sci. J. Koya Univ.*, vol. 11, no. 1, pp. 116–120, 2023.

[5] A. Rezaei, S. I. Yahya, and L. Nouri, "A high-performance microstrip bandpass filtering coupler with low-loss and compact size," *Microw. Opt. Technol. Lett.*, vol. 65, no. 9, pp. 2483–2487, Sep. 2023.

[6] K. Al-Majdi and Y. S. Mezaal, "New miniature narrow band microstrip diplexer for recent wireless communications," *Electronics*, vol. 12, no. 3, p. 716, Feb. 2023.

[7] C. Chen, B. Tseng, G. Wang, and J. Li, "Compact microstrip eight-channel multiplexer with independently switchable passbands," *IET Microw., Antennas Propag.*, vol. 12, no. 6, pp. 1026–1033, May 2018.

[8] S. I. Yahya, A. Rezaei, and L. Nouri, "Design and fabrication of a high-performance microstrip multiplexer using computational intelligence for multi-band RF wireless communications systems," *AEU-Int. J. Electron. Commun.*, vol. 120, Jun. 2020, Art. no. 153190.

[9] L. Nouri, S. I. Yahya, A. Rezaei, F. Hazzazi, M. A. Chaudhary, M. Assaad, and B. N. Nhu, "Microstrip lowpass-bandpass triplexer with flat channels and low insertion losses: Design and fabrication for multi-service wireless communication systems," *AEU-Int. J. Electron. Commun.*, vol. 170, Oct. 2023, Art. no. 154807.

[10] C. Zhu, J. Xu, W. Kang, and W. Wu, "Design of balun-integrated switchable low-pass-bandpass triplexer," *IEEE Microw. Wireless Compon. Lett.*, vol. 27, no. 4, pp. 353–355, Apr. 2017.

[11] F.-C. Chen, J.-M. Qiu, H.-T. Hu, Q.-X. Chu, and M. J. Lancaster, "Design of microstrip lowpass-bandpass triplexer with high isolation," *IEEE Microw. Wireless Compon. Lett.*, vol. 25, no. 12, pp. 805–807, Dec. 2015.

[12] J. Xu, Z.-Y. Chen, and H. Wan, "Lowpass–bandpass triplexer integrated switch design using common lumped-element triple-resonance resonator technique," *IEEE Trans. Ind. Electron.*, vol. 67, no. 1, pp. 471–479, Jan. 2020.

[13] A. Rezaei, S. I. Yahya, L. Noori, and M. H. Jamaluddin, "Design and fabrication of a compact microstrip triplexer for WiMAX and wireless applications," *Eng. Rev.*, vol. 41, no. 1, pp. 85–91, 2020.

[14] A. Rezaei and L. Noori, "Novel low-loss microstrip triplexer using coupled lines and step impedance cells for 4G and WiMAX applications," *TURKISH J. Electr. Eng. Comput. Sci.*, vol. 26, no. 4, pp. 1871–1880, Jul. 2018.

[15] C.-F. Chen, T.-M. Shen, T.-Y. Huang, and R.-B. Wu, "Design of multimode net-type resonators and their applications to filters and multiplexers," *IEEE Trans. Microw. Theory Techn.*, vol. 59, no. 4, pp. 848–856, Apr. 2011.

[16] A. Chinig, A. Errkik, L. E. Abdellaoui, A. Tajmouati, J. Zbitou, and M. Latrach, "Design of a microstrip diplexer and triplexer using open loop resonators," *J. Microw., Optoelectron. Electromagn. Appl.*, vol. 15, no. 2, pp. 65–80, Jun. 2016.

[17] A. Rezaei, S. I. Yahya, and L. Nouri, "Design and analysis of a compact microstrip lowpass–bandpass diplexer with good performance for wireless applications," *Int. J. Microw. Wireless Technol.*, vol. 15, no. 7, pp. 1099–1107, Sep. 2023.

[18] M. Hayati, A. Rezaei, and L. Noori, "Design of a high–performance lowpass–bandpass diplexer using a novel microstrip structure for GSM and WiMAX applications," *IET Circuits, Devices Syst.*, vol. 13, no. 3, pp. 361–367, May 2019.

[19] S. I. Yahya, F. Zubir, L. Nouri, A. Rezaei, F. Hazzazi, M. A. Chaudhary, M. Assaad, Z. Yusoff, and B. Nguyen Le, "A high-performance microstrip triplexer with compact size, flat channels and low losses for 5G applications," *IEEE Access*, vol. 11, pp. 78768–78777, 2023.

[20] M. Hayati, A.-R. Zarghami, S. Zarghami, and S. Alirezaee, "Designing a miniaturized microstrip lowpass-bandpass diplexer with wide stopband by examining the effects between filters," *AEU-Int. J. Electron. Commun.*, vol. 139, Sep. 2021, Art. no. 153912.

[21] S. Elden and A. K. Gorur, "Design of a compact lowpass-bandpass diplexer with high isolation," *Prog. Electromagn. Res. Lett.*, vol. 97, pp. 21–26, 2021.

[22] R. Jiang, W. Xie, S. Yan, J. Li, X. Zhang, Q. Meng, J. Dai, Y. Yuan, C. Zhang, J. Wang, C. Li, Y. Wu, X. Wang, and L. Sun, "Fabrication of C-band high-temperature superconducting microstrip triplexer with high accuracy," *Int. J. RF Microw. Comput.-Aided Eng.*, vol. 2023, pp. 1–7, Aug. 2023.

[23] Y. Liu, W.-B. Dou, and Y.-J. Zhao, "A tri-band bandpass filter realized using tri-mode T-shape branches," *Prog. Electromagn. Res.*, vol. 105, pp. 425–444, 2010.
[24] L. Nouri, S. Yahya, and A. Rezaei, "Design and fabrication of a low-loss microstrip lowpass-bandpass diplexer for WiMAX applications," *China Commun.*, vol. 17, no. 6, pp. 109–120, Jun. 2020.
[25] S.-C. Lin, "Microstrip dual/quad-band filters with coupled lines and quasi-lumped impedance inverters based on parallel-path transmission," *IEEE Trans. Microw. Theory Techn.*, vol. 59, no. 8, pp. 1937–1946, Aug. 2011.
[26] S. I. Yahya, F. Zubir, L. Nouri, Z. Yusoff, F. Hazzazi, M. A. Chaudhary, M. Assaad, A. Rezaei, and B. N. Le, "Design and optimization of a compact microstrip filtering coupler with low losses and improved group delay for high-performance RF communication systems," *IEEE Access*, vol. 11, pp. 103976–103985, 2023.

LEILA NOURI received the B.Sc. and M.Sc. degrees in electronic engineering from Razi University, Kermanshah, Iran, in 2005 and 2009, respectively, and the Ph.D. degree in electronic engineering from the Shiraz University of Technology. She is currently the author of one book, more than 60 articles, and more than five research and industrial projects. Her research interests include microstrip couplers, microstrip filters, neural networks, and LNAs.

FARID ZUBIR (Member, IEEE) received the B.Eng. degree in electrical (majoring in telecommunication) and the M.Eng. degree in RF and microwave from Universiti Teknologi Malaysia (UTM), in 2008 and 2010, respectively, and the Ph.D. degree from the University of Birmingham, U.K., in 2016, for research into direct integration of power amplifiers with antennas in microwave transmitters. He was an Honorary Postdoctoral Research Fellow with The University of British Columbia (UBCO), Okanagan, BC, Canada, from September 2019 to August 2021, where he conducted research into highly efficient and linear amplification power amplifier topology for wireless power systems. He is currently an Assistant Professor and a Research Fellow with the Department of Communication Engineering, School of Electrical Engineering, and the Wireless Communication Centre, UTM, respectively. His research interests and specialization include the area of RF and microwave technologies, including linearization and high-efficiency techniques for PAs, beamforming networks, planar array antenna, dielectric resonator antenna (DRA), and active integrated antenna (AIA).

LEWIS NKENYEREYE received the Ph.D. degree in information security from Pukyong National University, Busan, South Korea. He was a Research Fellow with the Creative Human Resource Development Program for IT Convergence, Pusan National University. He was a Visiting Scholar with Thompson Rivers University, Kamloops, BC, Canada, and Georgia Southern University, Statesboro, GA, USA. He is currently an Assistant Professor of computer and information security with the Department of Computer and Information Security, College of Electronics and Information Engineering, Sejong University, Seoul, South Korea. He is also involved in privacy-preserving techniques projects for blockchain-based applications, interoperability challenges in the IoT, and M2M standards (with a special focus on one M2M). His research spans across a wide range of security and privacy-related techniques with a particular interest in the Internet of Things (specifically the Internet of Vehicles). He has served as a member of several technical program committees in various conferences and journals.

ABBAS REZAEI was born in Kermanshah, Iran, in 1982. He received the B.S.E., M.S.E., and Ph.D. degrees in electronics engineering from Razi University, Kermanshah, in 2005, 2009, and 2013, respectively. He is currently an Associate Professor of electrical engineering with the Kermanshah University of Technology. He is the author of two books, more than 100 articles, and more than ten research and industrial projects. His current research interests include RF and microwave circuits and computational intelligence.

MOHAMMED ABDEL-HAFEZ (Senior Member, IEEE) received the B.Sc., M.Sc., and Ph.D. degrees in electrical and electronic engineering from Eastern Mediterranean University (EMU), Northern Cyprus, Turkey, in June 1992, August 1994, and November 1997, respectively. From 1992 to 1997, he was a Research Engineer with the Department of Electrical and Electronic Engineering, EMU. In 1995, he was an Instructor with the Department of Electrical Engineering, Al-Quds University. From 1997 to 1999, he was a Senior Manager with on the Manager with Palestine Telecommunications Company. In August 1999, he joined the Centre for Wireless Communications, University of Oulu, Oulu, Finland, as a Senior Research Scientist and a Project Manager. He is currently an Associate Professor of electrical and communication engineering with United Arab Emirates University, United Arab Emirates. He is also a Frequent Visiting Scientist with the Centre for Wireless Communications, University of Oulu. His research interests include modeling, design, and performance analysis of wireless communication systems, radio access, sensor networks, the IoT, cooperative and relay networks, NOMA, cognitive radio networks, advanced receivers' algorithms, and ultra-wideband (UWB) communication.

FAWWAZ HAZZAZI was born in Al-Kharj, Riyadh, Saudi Arabia. He received the Bachelor of Science (B.S.) degree in electrical engineering from the College of Engineering, Prince Sattam bin Abdulaziz University, Al-Kharj, the M.S. degree in electrical and computer engineering from The University of Maine, Orono, ME, USA, and the Ph.D. degree in electrical engineering from Louisiana State University, Baton Rouge, LA, USA. He has both industry and academic experience. His current research interests include the characterization and fabrication of nanomaterials for the production of nanoscale electronic applications and electronic sensors of the next generation.

MUHAMMAD AKMAL CHAUDHARY (Senior Member, IEEE) received the master's and Ph.D. degrees in electrical and electronic engineering from Cardiff University, Cardiff, U.K., in 2007 and 2011, respectively, and the M.B.A. degree in leadership and corporate governance from the Edinburgh Business School, Heriot-Watt University, Edinburgh, U.K., in 2022. Before joining Ajman University, United Arab Emirates, in 2012, he held a postdoctoral research position with the Centre for High-Frequency Engineering, Cardiff University. He is currently an Associate Professor of electrical engineering with Ajman University. His research interests include nonlinear device characterization, spectrum-efficient power amplifiers, nonlinear measurement techniques, and microwave electronics have resulted in more than 100 academic articles. He is a fellow of the Higher Education Academy, U.K. He is a Chartered Engineer of the Engineering Council, U.K.

MAHER ASSAAD received the master's degree in electrical engineering/microelectronics IC design from the University of Montreal, Montreal, Canada, in 2002, and the Ph.D. degree in electrical engineering/microelectronics IC design from the University of Glasgow, Glasgow, U.K., in 2009. He was a Senior Lecturer of electrical engineering with the University Technology of PETRONAS, Malaysia, and an Associate Professor of electronic and communication engineering with the American University of Ras Al Khaimah, United Arab Emirates. He is currently a Professor of electrical and computer engineering with Ajman University, United Arab Emirates. His research interests include the design of circuits/integrated circuits for various types of sensors and wireline and optical communication systems.

ZUBAIDA YUSOFF (Senior Member, IEEE) received the B.Sc. degree (cum laude) in electrical and computer engineering and the M.Sc. degree in electrical engineering from The Ohio State University, USA, in 2000 and 2002, respectively, and the Ph.D. degree from Cardiff University, Wales, U.K., in 2012. She was with Telekom Malaysia International Network Operation, in 2002, before she joined Multimedia University, in 2004. She holds the position of a senior lecturer with the Faculty of Engineering, Multimedia University. She has presented technical papers at conferences nationally and internationally. She has authored/coauthored more than 50 journals and conference papers. Her teaching and research focus on the area of power amplifier design, antenna, 5G communications, and analog/mixed-signal RF circuit design. One of her conference papers has received ''Honorable Mention'' for the Student Paper Competition from the International Microwave Symposium, USA, in 2011.